Transactions on the Built Environment vol 71, © 2004 WIT Press, www.witpress.com, ISSN 1743-3509

An Eulerian-Lagrangian approach for large deformation fluid structure interaction problems, Part 1: algorithm development

J.E. Guilkey[1], T.Harman[1], A. Xia[1], B. Kashiwa[2], &
P. McMurtry[1]
[1] *Dept. of Mechanical Engineering, University of Utah, Salt Lake City, USA*
[2] *Theoretical Division, Los Alamos National Laboratory, Los Alamos, USA*

Abstract

A numerical algorithm for tightly coupled, high-deformation fluid-structure interaction problems is presented. The foundation of the method is the integration of a Lagrangian particle technique (the Material Point Method, or MPM) with a multi-material Eulerian code. In this approach, each material is described and evolves in its preferred reference frame (e.g., Lagrangian for solids, Eulerian for fluids). The MPM uses a background mesh to update particle states. By using the Eulerian multi-material mesh as the background mesh to update particle states, the solid materials have a dual representation in the Lagrangian and Eulerian frame. It is in this common reference frame that coupling interactions among materials are computed through momentum and energy exchange terms in the multi-field equations. The approach is outlined and results from a numerical order-of-accuracy study are presented. Simulation results are compared with known solutions for the stress distribution in a pressurized cylinder. It is shown that the combined approach has the same order-of accuracy as the stand-alone material point method and gives excellent agreement with exact solutions for this geometry.

1 Introduction

The work presented here describes a new approach for "full physics" simulations of fluid-structure interactions involving large deformations and phase change. By "full physics" we refer to problems involving strong coupling between the fluid and solid phases with a full Navier-Stokes representation of fluid phase materials and the transient, nonlinear response of solid phase materials, which may include chemical or phase transformation between the solid and fluid phases.

Although a general classification of numerical approaches for "full physics" FSI problems has not been consistently reported, most involve an arbitrary Lagrangian-Eulerian (ALE) representation of the fluid, a Lagrangian representation of the solid and either a simultaneous or partitioned solution approach. Explicit representation of the boundary conditions between the different materials is required in the numerical solution in these approaches as interaction is generally only allowed at the boundaries. Examples of such approaches are widespread, (see [1, 2, 3, 4, 5]).

A second class of approach can be identified where surface tracking is used to distinguish the interface between the two materials. In such techniques, most of the computational cells contain either one material or the other, with a minority of cells that contain the interface between materials. This is a widely used approach for mixed material problems. The multi-material simulations of the microstructure of heterogeneous materials described by Benson[6, 7] fall into this class.

Another methodology, built upon here, is a full "multi-field" approach in which each material is given a continuum description and defined over the complete computational domain. Although at any point in space the material composition is uniquely defined, the multi-field approach adopts a statistical viewpoint whereby the material (either fluid or solid) resides with some finite probability. To determine the probability of finding a particular material at a specified point in space, together with its current state (i.e., mass, momentum, energy), multi-field equations are used. This paper describes an algorithm that uses a common framework to treat the coupled response of a collection of arbitrary materials. This follows the ideas previously presented by Kashiwa and coworkers.[8, 9]

The remainder of this paper is organized as follows: In Sec. 2, the FSI algorithm that is studied here is presented. This includes a description of the multi-field equations that form the foundation of the approach. A unique aspect of the approach is the ability to describe any of the chosen materials in either an Eulerian or Lagrangian frame. For solid phase materials, we use an updated Lagrangian approach known as the Material Point Method (MPM). This is discussed in Sec. 2.3. The multi-field equations (representing both fluid and solid fields) are developed and will be implemented using a cell-centered, Eulerian finite volume technique. The solid field variables, described in the Lagrangian MPM technique, also are represented in the Eulerian multi-field equations. This multi-reference frame description is a unique feature and key to using the multi-field approach for large deformation FSI problems. How this integration is accomplished is described in Sec. 2.4. A sample validation calculation is shown in Sec. 3. Further validation and demonstration calculations are shown in Part 2 of this paper [10].

2 FSI coupled algorithm description

The FSI method described here involves integrating a Lagrangian particle method (see Sec. 2.3) into a general multi-material Eulerian formulation. A description of the various elements that make up this approach follows.

2.1 The multi-field (material) equations

The objective of our FSI efforts is to develop a general computational approach that can treat interactions among multiple materials that have widely varying thermodynamic and mechanical response. A logical starting point is then the general continuum equations for a mixture of materials. For this application, it is assumed that at any point in space a material can be uniquely defined. For the purpose of developing the multi-field equations, however, the derivation invokes a probabilistic approach in which a particular material in a multi-material field exists in any finite region with a determined probability. In this description, material interfaces are not explicitly defined, although the complete approach proposed here can account for material interfaces when proper treatment of the physics necessitates this resolution. The general multi-material equations are [11]:

$$\frac{\partial \rho^r}{\partial t} = -\frac{\partial (\rho u_j)^r}{\partial x_j} + \sum_{n=1, n\neq r}^{N} S_{\rho}^{r\leftrightarrow n} \tag{1}$$

$$\frac{\partial (\rho u_i)^r}{\partial t} + \frac{\partial (\rho u_i u_j)^r}{\partial x_j} = \theta^r \frac{\partial \sigma_{ij}}{\partial x_j} + \frac{\partial}{\partial x_j}\theta^r(\sigma_{ij}^r - \sigma_{ij}) + \sum_{s=1}^{N} f_{sr} + \sum_{n=1, n\neq r}^{N} S_{\rho u}^{r\leftrightarrow n} \tag{2}$$

$$\frac{\partial (\rho e)^r}{\partial t} + \frac{\partial (\rho e u_j)^r}{\partial x_j} = -p\left(\theta\rho \frac{D(1/\rho)}{Dt}\right)^r + \theta^r(\sigma_{ij}^r - \sigma_{ij})\frac{\partial u_i^r}{\partial x_j} + \theta^r \tau_{ij}\frac{\partial u_i^r}{\partial x_j} + \sum_{s=1}^{N} h_{sr} + \sum_{n=1, n\neq r}^{N} S_{\rho e}^{r\leftrightarrow n} \tag{3}$$

Equations 1 - 3 represent the conservation equations of mass, momentum, and energy for material r, where $r = 1, 2, ..., N$ and N is the total number of materials present. ρ^r, u^r, e^r, θ^r and σ^r represent the r-material density (r-material mass per unit volume), velocity, internal energy, volume fraction and stress, respectively. $\boldsymbol{\sigma}$ (without the material specific superscript) is the mean total stress over all materials, $\boldsymbol{\tau}$ is the mean deviatoric stress. In the current work, $\boldsymbol{\sigma}$ is assumed to be equal to the pressure, (i.e. $\boldsymbol{\sigma} = p\mathbf{I}$), in which case, $\boldsymbol{\tau}$ vanishes. As written, Eq. 2 is missing any representation of the r-material momentum flux, otherwise known as the multi-material Reynolds Stress. Similarly, Eq. 3 contains no representation of the r-material fluctuational energy flux. Neither of these terms, which must be

modeled, was considered in the current work, and so they are not included in the above equations.

In Eq. 2 the term $\sum_{s=1}^{N} f_{sr}$ represents a model for the momentum exchange among materials. This term results from the deviation of the r-material stress from the mean stress, $\sigma'_{ij}\frac{\partial}{\partial x_j}\alpha_r$. This is typically modeled as a function of the relative velocity between materials at a point (e.g. for a two material problem this term might look like $f_{12} = K_{12}\theta^1\theta^2(u^2 - u^1)$ where K_{12} determines the rate at which momentum is transferred between materials). Likewise, in Eq. 3, $\sum_{s=1}^{N} h_{sr}$ represents an exchange of internal energy among materials and for a two material problem typically takes the form $h_{12} = H_{12}\theta^1\theta^2(T^2 - T^1)$ where T^r is the r-material temperature and H_{sr} is somewhat analogous to a convective heat transfer coefficient.

The terms $S_p^{r\leftrightarrow n}$, $S_{\rho u}^{r\leftrightarrow n}$ and $S_{\rho e}^{r\leftrightarrow n}$ in Eqs. 1 - 3, respectively, represent contributions to those equations due to phase conversion. Discussion of phase change is contained in Part 2 of this work, Harman et al. [10]

Given appropriate constitutive models and equations of state, along with proper models for the momentum and energy exchange, the above equations can, in theory, be solved for the evolution of the state of the N materials. These equations, or similar variants have appeared much earlier (the 1960's) in various multi-phase and mixture-theory relations. Their general numerical solution for an arbitrary mixture of materials has met with less success. One difficulty for fluid-structure interaction simulations using purely Eulerian finite volume technique is the unacceptable diffusion of solid boundaries. This can be alleviated with careful surface tracking approaches. This paper describes a different approach. This involves invoking either an Eulerian *or* Lagrangian frame to describe individual materials. Specifically, the frames of reference can be mixed in an integrated solution approach. (See Sec. 2.4.)

2.2 Multi-field CFD approach

The multi-field CFD formulation used here is a cell-centered, multimaterial version of the ICE (for Implicit, Continuous-fluid, Eulerian) method [12] developed by Kashiwa and others at Los Alamos National Labs[13]. The use of a cell centered approach is convenient for multi-material simulations in that a single control volume is used for all materials. This is particularly important in regions where a material volume goes to zero. By using the same control volume for mass and momentum it can be assured that as the material volume goes to zero, the mass and momentum go to zero at the same point. The technique is fully compressible, allowing wide generality in the types of problems that can be efficiently computed.

Our implementation of the ICE technique invokes operator splitting in which the solution consists of a separate Lagrangian phase where the physics of the conservation laws is computed (e.g., right hand side of Eqs. 2-3), and an Eulerian phase, where the material state in each cell is updated with contributions fluxed into and out of surrounding cells. The general solution approach is well developed and described in [13]. Where appropriate, details specific to the solution of FSI

Transactions on the Built Environment vol 71, © 2004 WIT Press, www.witpress.com, ISSN 1743-3509

problems are expounded upon in Sec. 2.4.

A physical and numerical requirement of this multi-material approach is that the total volume fraction of material must sum to one in each cell. This can be enforced by equating the mean stress, σ, with an *equilibrium* pressure, p_{eq}, defined as the common material isotropic stress at a point such that the volume fractions of the materials sum to 1. This common equilibrium pressure can be determined through a multi-material equation of state. Specifically, the volume fraction, $\theta^r = \rho^r v^r(p)$. v^r is the specific volume of material r and is a function of pressure. Therefore, the pressure can be determined in an iterative process such that:

$$\sum_{r=1}^{N} \theta^r = \sum_{r=1}^{N} \rho^r v^r(p) = 1 \tag{4}$$

Equation 4 can be considered a multi-material equation of state that ensures the volume fraction of materials always adds up to 1. This approach is unambiguous when all materials are fluids or in cases of a multi-phase flow consisting of dispersed particles in a carrier fluid. However, when considering fluid-structure problems, the interpretation of a common equilibrium pressure can be troublesome. The case of a solid in tension in a gas (which can only be in compression) is a clear case. For solid materials, the equation of state is just the bulk part of the constitutive response. The problem encountered with this approach is that when the hydrostatic stress in the solid gives a negative pressure, Eq. 4 is not solvable. To overcome this obstacle, the solid material equation of state is altered such that, below a particular threshold pressure (typically one atmosphere), the pressure obeys a polynomial chosen to be continuous and smooth at the threshold value and also approaches zero as the specific volume becomes large. While this may seem like a reckless alteration of the material behavior to achieve the desired result, it's logical justification is fairly straightforward.

First, in regions where a mixture of solid and fluid coexist, the high compressibility of the fluid causes it's behavior to dominate the solution of Eq. 4, and thus the regime of negative pressure is never encountered. Furthermore, examination of Eq. 2 reveals that this issue is of no importance in regions containing either pure fluid or pure solid since, in those regions, the two terms containing the mean stress cancel, leaving only the contribution from the r-material stress. An example of just such a situation, with a fluid in compression and a solid in tension is demonstrated in Sec. 3.

2.3 The material point method

A novel feature of the complete multi-material algorithm developed here is the ability to describe solid phase and fluid phase materials in different reference frames (Eulerian or Lagrangian), while maintaining a tight coupling through a general multi-field formulation. The achievement of this tight coupling through a unified multi-material framework is described in Sec. 2.4. Here, we first describe the material representation in the Lagrangian material point frame. In the Lagrangian

frame the state variables of the material are described on "material points." The numerical technique used is the Material Point Method (MPM). Specifically, the Material Point Method, described by Sulsky, et al. [14, 15] is a particle method for structural mechanics simulations. The method generally uses a regular structured grid as a computational scratchpad for computing spatial gradients. This same grid also functions as an updated Lagrangian grid that moves with the particles during advection and thus eliminates the diffusion problems associated with advection on an Eulerian grid. At the end of a timestep, the grid is reset to the original regularly ordered position.

In explicit MPM, the equations of motion are cast in the form [15]:

$$\mathbf{M}_g \cdot \mathbf{a}_g = \mathbf{Fext}_g - \mathbf{Fint}_g \tag{5}$$

where $\mathbf{M}_g$ is the mass matrix, $\mathbf{a}_g$ is the acceleration vector, $\mathbf{Fext}_g$ is the external force vector (sum of the body forces and tractions), and $\mathbf{Fint}_g$ is the internal force vector resulting from the divergence of the material stresses.

The solution procedure begins by interpolating the particle state to the grid, to form $\mathbf{M}_g$, $\mathbf{Fext}_g$, and to determine a velocity on the grid $\mathbf{v}_g$. In practice, a lumped mass matrix is usually used. These quantities are calculated by the following equations:

$$\mathbf{M}_i = \sum_p S_{ip} m_p, \qquad \mathbf{v}_i = \frac{\sum_p S_{ip} m_p \mathbf{v}_p}{\mathbf{M}_i}, \qquad \mathbf{Fext}_i = \sum_p S_{ip} \mathbf{Fext}_p \tag{6}$$

where i refers to individual nodes of the grid. m_p is the particle mass, $\mathbf{v}_p$ is the particle velocity, and $\mathbf{Fext}_p$ is the external force on the particle. S_{ip} is the ith node's trilinear shape function evaluated at $\mathbf{x}_p$.

At this point, a velocity gradient, $\nabla \mathbf{v}_p$ is computed at the particle using the velocities interpolated to the grid:

$$\nabla \mathbf{v}_p = \sum_p \mathbf{G}_{ip} \mathbf{v}_i \tag{7}$$

where $\mathbf{G}_{ip}$ is the gradient of the ith nodes shape function, evaluated at $\mathbf{x}_p$.

This is used as input to a constitutive model which is evaluated on a per particle basis, the result of which is the Cauchy stress at each particle, $\boldsymbol{\sigma}_p$. With this, the internal force due to the divergence of the stress is calculated via:

$$\mathbf{Fint}_i = \sum_p \mathbf{G}_{ip} \boldsymbol{\sigma}_p v_p, \tag{8}$$

where v_p is the particle volume.

Transactions on the Built Environment vol 71, © 2004 WIT Press, www.witpress.com, ISSN 1743-3509

Equation 5 can then be solved for $\mathbf{a}_g$. An explicit backward Euler method is used for the time integration. The particle position and velocity is explicitly updated by:

$$\mathbf{v}_p(t+dt) = \mathbf{v}_p(t) + \sum_i S_{ip}\mathbf{a}_i dt \tag{9}$$

$$\mathbf{x}_p(t+dt) = \mathbf{x}_p(t) + \sum_i S_{ip}\mathbf{v}_i^L dt \tag{10}$$

This completes one timestep. In addition to the basic algorithm outlined above, the MPM makes convenient the modeling of several important processes. Among these is contact between solid bodies, which has traditionally been difficult. The difficulties stem from both the proper specification of the physics and the numerical solution constraint inequalities. In MPM, many of the computational difficulties are removed by describing contact on the background mesh. A detailed description of the contact algorithm is beyond the scope of this paper, but can be found in [16].

2.4 Integration of the Material Point Method in an Eulerian multi- material formulation

The key feature of this work is the development, demonstration, and validation of a tightly coupled solution approach that allows simulations of arbitrary materials undergoing arbitrary physical and chemical processes. Fundamental to the proposed approach is the representation of a material field in either an Eulerian or Lagrangian reference frame, all while working within a general multi-field continuum description. This allows treating specific phases in their traditionally preferred frame of reference, Lagrangian for solid, Eulerian for fluid. While reference is made to "coupling" an MPM code to a CFD code, **it needs to be recognized that this is much different than the marriage of two distinct codes via boundary conditions.** Here, we have chosen to use the MPM algorithm, which uses particles along with an updated Lagrangian description of the solid material on the grid, to time advance those materials which are best described in that reference frame. However, by choosing the background mesh used to update the MPM materials, to be one and the same as the mesh used in the multi-material Eulerian description, all interactions among materials can be enforced to occur in the common framework.

Specifically, all materials, solid or fluid, will have a presence in the Eulerian description. This common reference frame is used for all physics that involve mass, momentum, or energy exchange among materials. This allows for a tight coupling between the fluid and solid phases. **The coupling occurs through terms in the conservation equations, rather than explicitly through specified boundary conditions at interfaces between materials.** *Since a common multi-field Eulerian frame is used for interactions among materials, typical problems with convergence and stability of solutions for separate domains communicating only through boundary conditions are alleviated.* All solid phase materials thus have a dual representation - in both the Lagrangian (MPM) and Eulerian framework.

It is primarily in advection, as well as in the computation of internal forces, that the use of the separate reference frames becomes important. Eulerian advection is typically subject to significant diffusion. Therefore if the Eulerian frame is used exclusively for both solid and fluid materials, the interface between the materials will become smeared and nonphysical behavior may result. The use of a particle description for the solid advection minimizes this problem. Furthermore, while straining history does not typically play a role in the stress field in a fluid, it is important in many engineering solid materials to describe phenomenon such as plasticity. The particle description of the solid provides a convenient frame to evaluate the solid material stress, and to store and carry forward in time the relevant history variables. This role of the particle is similar to the role that Gaussian integration points play in finite element method formulations. On the other hand, if a particle description is used for fluid phases, the random behavior of general fluid motion will generally result in very random particle distributions. This limits the utility of the MPM for fluid calculations. However, the integration of the two, where part of the calculation takes place in a common reference frame, allows each material phase to enjoy it's optimum description and achieves a tight coupling.

What follows is the explicit algorithm for advancing a fluid-solid problem.

1. **Interpolate Particle state to grid** Interpolate the particle description of the solid to the grid, so that all materials are described in a common frame of reference. This starts with an interpolation of particle data to grid vertices, or nodes, as described in Eq. 6, and is followed by a subsequent interpolation from the nodes to the cell centers. Since our work uses a uniform structured grid, each node has equal weight in it's contribution to the cell centered value. The exception to this is near computational boundaries. For instance, if symmetric boundary conditions are used, the weight of those nodes on the boundary must be doubled in order to achieve the desired effect.

2. **Compute the equilibrium pressure** While Eq. 4 and the surrounding discussion describes the basic process, a few specifics warrant further explanation. In particular, the manner in which each material's volume fraction is computed is crucial. Typically, in multi-field CFD calculations, this would simply be the material volume divided by the cell volume. However, because the solid and fluid materials are advected in different manners (see below) the total volume of material in a cell is not necessarily equal to the volume of a computational cell. Because of this, it is important to have an accurate accounting of the volume of material in each cell. This is done by solving the evolution equation for each material's specific volume given in step 11.

   With the materials' masses and specific volumes in hand, material volume can be computed and summed to find the total material volume. The volume fraction θ^r is then computed as the volume of r-material per total material volume. With this, the solution of Eq. 4 can be carried out at each cell using a Newton-Raphson technique[17], which results in new values for the equilibrium pressure, p_{eq}, volume fraction, θ^r and specific volume, v^r.

3. **Compute face centered velocities, u^{*^f}, for the Eulerian advection** This includes adjusting the face centered velocities to account for momentum exchange between all N-materials. Specific details associated with this step are given in [13] and [11].

4. **Multiphase chemistry** Compute sources of mass, momentum and energy as a result of phase changing chemical reactions, $S_\rho^{r\leftrightarrow n}$, $S_{\rho u}^{r\leftrightarrow n}$, and $S_{\rho e}^{r\leftrightarrow n}$. Details of this are described in [10].

5. **Compute an estimate of the time advanced pressure, P** Based on the face centered fluxing velocities and the material properties, an increment in the pressure due to the motion of material is computed via:

$$\Delta P = -\Delta t \frac{\sum_{r=1}^{N} \nabla \cdot (\theta u^*)^r}{\sum_{r=1}^{N} (\theta \kappa)^r} \tag{11}$$

where κ^r is the r-material bulk compressibility.

Again, specific details of this calculation can be found in [13]. Additional contributions to the pressure increment resulting from phase conversion are described in [10].

6. **Face Centered Pressure P^{*^f}** The calculation of P^{*^f} is discussed at length in [11]. For this work, it is computed using the updated pressure by:

$$P^{*^f} = (\tfrac{P_L}{\rho_L} + \tfrac{P_R}{\rho_R})/(\tfrac{1}{\rho_L} + \tfrac{1}{\rho_R})$$

This will be used subsequently for the computation of the pressure gradient, ∇P^{*^f}.

7. **Material Stresses** For the solid, we calculate the velocity gradient at each particle based on the grid velocity (Eq. 7) for use in a constitutive model to compute particle stress. Fluid stresses are computed on cell faces based on cell centered velocities.

8. **Accumulate sources of mass, momentum and energy at cell centers** These terms are of the form:

$$\Delta(m)^r = \sum_{n=1, n\neq r}^{N} S_\rho^{r\leftrightarrow n}$$

$$\Delta(mu)^r = -\Delta t V \theta^r \nabla P^{*^f} + \nabla \cdot \theta^r (\boldsymbol{\sigma}^r - \boldsymbol{\sigma}) + \textstyle\sum_{n=1, n\neq r}^{N} S_{\rho u}^{r\leftrightarrow n}$$

$$\Delta(me)^r = -\Delta t V f_r^\theta P \sum_{r=1}^{N} \nabla \cdot (\theta u^*)^r + \sum_{n=1, n\neq r}^{N} S_{\rho e}^{r\leftrightarrow n}$$

where f_r^θ is a measure of the relative compressibility of the r-material in a cell. Specifically, $f_r^\theta = \frac{\theta^r \kappa^r}{\sum_{s=1}^{N} \theta^s \kappa^s}$.

9. **Compute Lagrangian phase quantities at cell centers**

$$(m)^{r^{L-}} = (m)^{r^n} + \Delta(m)^r$$
$$(mu)^{r^{L-}} = (mu)^{r^n} + \Delta(mu)^r$$
$$(me)^{r^{L-}} = (me)^{r^n} + \Delta(me)^r$$

10. **Momentum and heat exchange** The last step in the Lagrangian phase is the exchange of momentum and heat between materials.

$$(mu)^{r^L} = (mu)^{r^{L-}} + \Delta t m^r \sum_{s=1}^{N} \theta^r \theta^s K_{rs}(u^{s^L} - u^{r^L})$$
$$(me)^{r^L} = (me)^{r^{L-}} + \Delta t m^r c_v^r \sum_{s=1}^{N} \theta^r \theta^s R_{rs}(T^{s^L} - T^{r^L})$$

These equations are solved in a pointwise implicit manner that allows arbitrarily large momentum transfer to take place between materials. Typically, in FSI solutions, very large (10^{15}) values of K are used, which results in driving contacting materials to the same velocity. Intermaterial heat exchange typically modeled at a lower rate.

11. **Specific volume evolution** In order to accurately compute the equilibrium pressure, it is important to keep an accurate accounting of the specific volume. Here, we compute the evolution in specific volume due to the changes in temperature and pressure during the foregoing Lagrangian phase of the calculation, according to:

$$\Delta(mv)^r = \Delta t f_r^\theta V \nabla \cdot \sum \theta^{r^*} u^{r^{*^f}} + \Delta t V[\theta^r \alpha^r \dot{T}^r - f_r^\theta \sum \theta^s \alpha^s \dot{T}^s]$$

$$(mv)^{r^L} = (mv)^r + \Delta(mv)^r$$

where α is the constant pressure thermal expansivity and $\dot{T} = \frac{T^L - T^n}{\Delta t}$ is the rate of change of each material's temperature during the Lagrangian phase of the computation. The foregoing equations do not account for phase change effects. These will be described in [10].

12. **Advect Fluids** For the fluid phase, use a suitable advection scheme, such as that described in [18], to move fluid material between cells. This includes the transport of mass, momentum, internal energy and specific volume. As this last item is an intensive quantity, it is converted to material volume for advection, and then reconstituted as specific volume for use in the subsequent step's equilibrium pressure calculation.

13. **Advect Solids** For the solid phase, interpolate the time advanced grid velocity and the corresponding velocity increment back to the particles, and use these to advance the particle's position and velocity, respectively. This constitutes advection of the solid phase material.

This completes one timestep. In the preceding, the user has a number of options in the implementation. In ours, we first started with a working MPM code and a separate working multimaterial CFD code. It was our desire that in the coupling of the two algorithms, each of the original codes be able to stand on their own. Thus, for instance, in step 8 above, for the solid material we've chosen not to aggregate all of the momentum sources at the cell centers. Rather, the pressure gradient and mean pressure are computed at the cell centers, and interpolated back to the nodes, where the integration of the MPM equations normally take place. The time advanced solid material momentum is then aggregated at the cell centers for momentum exchange, and the resulting change in momentum is propagated back to the nodes and eventually the cell centers.

Again, we emphasize that the coupling of the MPM to the CFD simulation is readily achieved because of our use of a regular mesh for the gradient calculations in MPM. The grid thus serves as both an Eulerian reference frame for CFD calculations and an updated Lagrangian reference frame for MPM calculations.

3 Validation: stress distribution in a pressurized cylinder

To demonstrate the ability of the approach to accurately represent the interaction between fluid and solids, a cylinder of finite thickness is pressurized internally and the subsequent stress distribution in the cylinder is presented. The configuration is shown in Fig. 1. A uniform mesh is used and the solid cylinder is represented by material points as shown. The cylinder is made of steel with bulk and shear modulus of 117.0 GPa and 43.8 GPa respectively. Density is 8900 kg/m^3. Inner radius, r_i, is .5 m and outer radius, r_o, is 1.0 m. Although code capabilities are fully three dimensional, this example is two dimensional, with plane strain being the out of plane condition. As shown in Fig. 1 a one-quarter symmetric section of the cylinder was simulated. The fluid is defined everywhere on the mesh, although the volume fraction of the fluid is set to zero in the region occupied by the solid. Pressurization of the cylinder is achieved by adding internal energy to the fluid inside the cylinder over the course of 500 timesteps. The final pressure of 19.4 MPa then remains constant and viscous damping is used in the solid phase to achieve a quasi-static solution.

The exact solutions for the radial and circumferential stresses are given by [19] (where P is the pressure inside the container):

$$\sigma_r = \frac{Pr_i^2}{(r_o^2 - r_i^2)}\left(1 - \frac{r_o^2}{r^2}\right) \qquad \sigma_\theta = \frac{Pr_i^2}{(r_o^2 - r_i^2)}\left(1 + \frac{r_o^2}{r^2}\right) \tag{12}$$

The predicted stress distributions, computed using a grid spacing of .025 m in each direction, are compared to the exact solution in Fig. 2a. The agreement is

seen to be very good. It is particularly noteworthy that in the solution, there is no explicit representation of a surface or explicit description of surface tractions on the material points describing the cylinder. Coupling occurs completely through terms in the momentum equation (Eq. 2).

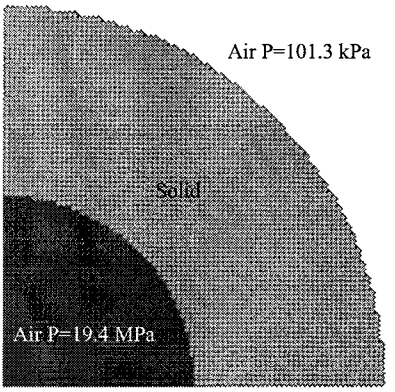

Figure 1: Initial configuration for pressurization of an annulus. The cylinder is described by material points on the Eulerian mesh of the multi-material solution.

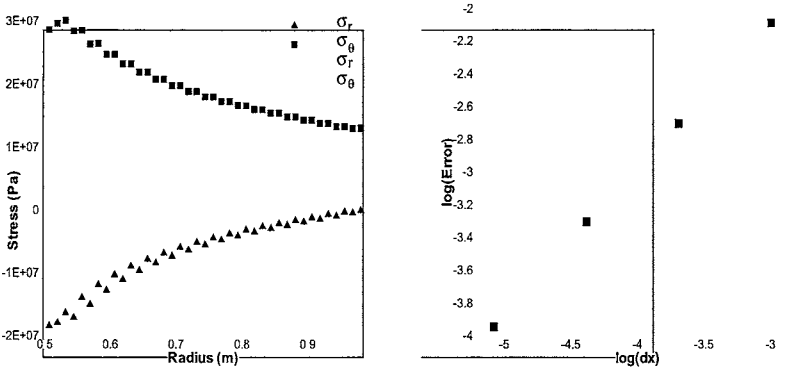

a b

Figure 2: Results from pressurization of an annulus, (a) radial and circumferential stresses, compared to the theoretical solutions, of the row of particles nearest the x-axis, and (b) natural log of solution error, averaged over all particles, vs. natural log of grid spacing. The slope of the line fit to the four data points indicates an order of accuracy of .89.

This simulation was carried out at several grid resolutions in order to characterize the order of accuracy of this algorithm. The error for each resolution was computed by:

$$Error = \frac{1}{N}\sum_{N}\frac{||\sigma_r + \sigma_\theta| - \frac{2}{3}P|}{\frac{2}{3}P} \tag{13}$$

Results from that are shown in Fig. 2b. When plotted in this log-linear manner, the slope of the straight line that best approximates these points indicates the order of accuracy. Here, a slope of .89 is found.

Acknowledgments

This work was supported by the National Science Foundation's Information Technology Research Program under grant CTS0218574, and the U.S. Department of Energy through the Center for the Simulation of Accidental Fires and Explosions, under grant W-7405-ENG-48. Los Alamos National Laboratory is operated by the University of California for the United States Department of Energy under contract W-7405-ENG-36; partial support from the Procter & Gamble Company, and from DOE Office of Industrial Technologies, is gratefully acknowledged.

References

[1] Lewis, M., Kashiwa, B., Meier, R. & Bishop, S., Nonlinear dynamic fluid-structure interaction calculations with coupled finite element and finite volume schemes. *ASME Winter Annual Meeting*, Chicago, IL, 1994.

[2] Bhardwaj, M., Kapania, R., Reichenbach, E. & Guruswamy, G., Computational fluid dynamics/computational structural dynamics interaction methodology for aircraft wings. *AIAA Journal*, **36**, pp. 2179–2186, 1998.

[3] Benney, R. & Stein, K., Computational fluid-structure interaction model for parachute inflation. *Journal of Aircraft*, **33**, pp. 730–736, 1996.

[4] Rugonyi, S. & Bathe, K., On finite element analysis of fluid flows fully coupled with structural interactions. *CMES*, **2**, pp. 195–212, 2001.

[5] Bathe, K., Zhang, H. & Ji, S., Finite element analysis of fluid flows coupled with structural interactions. *Computers & Strctures*, **72**, pp. 1–16, 1999.

[6] Benson, D.J., A multi-material Eulerian formulation for the efficient solution of impact and penetration problems. *Comput Mech*, **15**, pp. 558–557, 1995.

[7] Benson, D.J., Eulerian finite element methods for the micromechanics of heterogeneous materials: Dynamic prioritization of material interfaces. *Comput Methods Appl Mech Engrg*, **151**, pp. 343–360, 1998.

[8] Kashiwa, B.A. & Rauenzahn, R.M., A multimaterial formalism. Technical Report LA-UR-94-771, Los Alamos National Laboratory, Los Alamos, 1994.

[9] Kashiwa, B.A., Lewis, M.L. & Wilson, T., Fluid-structure interaction modeling. Technical Report LA-13111-PR, Los Alamos National Laboratory, Los Alamos, 1996.

[10] Harman, T., Guilkey, J.E., Schmidt, J., Kashiwa, B.A. & McMurtry, P., An Eulerian-Lagrangian approach for large deformation fluid structure interaction problems, part 2: Multi-physics simulations. *Proceedings of the Second International Conference on Fluid Structure Interaction*, Cadiz, Spain, 2003.

[11] Kashiwa, B., A multified model and method for fluid-structure interaction dynamics. Technical Report LA-UR-01-1136, Los Alamos National Laboratory, Los Alamos, 2001.

[12] Harlow, F.H. & Amsden, A.A., Numerical calculation of almost incompressible flow. *J Comp Phys*, **3**, pp. 80–93, 1968.

[13] Kashiwa, B.A. & Rauenzahn, R.M., A cell-centered ice method for multiphase flow simulations. Technical Report LA-UR-93-3922, Los Alamos National Laboratory, Los Alamos, 1994.

[14] Sulsky, D., Chen, Z. & Schreyer, H.L., A particle method for history-dependent materials. *Comp Methods Appl Mech Engrg*, **118**, pp. 179–196, 1994.

[15] Sulsky, D., Zhou, S. & Schreyer, H., Application of a particle-in-cell method to solid mechanics. *Computer Physics Communications*, **87**, pp. 236–252, 1995.

[16] Bardenhagen, S., Guilkey, J., Roessig, K., Brackbill, J., Witzel, W. & Foster, J., An improved contact algorithm for the material point method and application to stress propagation in granular material. *CMES*, **2**, pp. 509–522, 2001.

[17] Harlow, F.H. & Amsden, A.A., Flow of interpenetrating material phases. *J Comp Phys*, **18**, pp. 440–464, 1975.

[18] VanderHeyden, W.B. & Kashiwa, B., Compatible fluxes for van leer advection. *J Comp Phys*, **146**, pp. 1–28, 1998.

[19] Cook, R. & Young, W., *Advanced Mechanics of Materials*. Macmillan: New York, 1985.